February 2024

M.S. Dissertation

Multifunctional properties of symmetric tryptophan-rich antimicrobial peptides

Graduate School of Chosun University

Department of Biomedical Sciences

Bobin Choi

Multifunctional properties of symmetric tryptophan-rich antimicrobial peptides

다기능적인 특성을 갖는 트립토판이 풍부한
대칭－항균펩타이드 연구

2024년 2월 23일

Graduate School of Chosun University

Department of Biomedical Sciences

최보빈

Multifunctional properties of symmetric tryptophan-rich antimicrobial peptides

Advisor: Prof. Sungtae Yang

This dissertation is submitted to the Graduate School of Chosun University in partial fulfillment of the requirements for the degree of Master of Science

October 2023

Graduate School of Chosun University

Department of Biomedical Sciences

Bobin Choi

M.S. Dissertation of

Bobin Choi is certified by

Chairman	**Song Yub Shin**	.....
Committee Members	**Sung-Heui Shin**	.....
Committee Members	**Sungtae Yang**	.....

December 2023

Graduate School of Chosun University

CONTENTS

LIST OF TABLES

LIST OF FIGURES

초록

다기능적인 특성을 갖는 트립토판이 풍부한 대칭-항균펩타이드 연구

최보빈
지도교수: 양성태, Ph.D.
의과학과
조선대학교 대학원

항균 펩타이드(AMP)는 선천 면역계의 중요한 구성 요소이며 미생물 감염으로부터 숙주를 보호하는데 중요한 역할을 한다. 다양한 항균 펩타이드 중에 트립토판이 풍부한 대칭 항균 펩타이드(STRAMP)는 대칭 구조와 트립토판 잔기의 함량이 매우 높다. STRAMP는 작은 크기에도 불구하고 강력하고 광범위한 항균 활성을 갖는다. 본 연구에서는 항균, 항바이오필름 및 항염증 기능에 초점을 맞춰 독특한 구조적 특징을 가진 세 개의 STRAMP를 설계하고 합성하였다. 이러한 STRAMP는 메티실린 내성 황색포도상구균 (MRSA)과 다제내성 녹농균 (MDRPA)을 포함한 다양한 미생물에 대해 강력한 항균 효과를 나타내었다. 특히, 이 펩타이드들은 바이오필름 형성을 억제하였을 뿐만 아니라 형성된 바이오필름을 효과적으로 제거했다. 또한, STRAMP는 지질다당류 자극 대식세포에서 사이토카인 발현 수준을 크게 감소시킴으로써 항염증 효과를 보였다. 본 연구 결과는 STRAMP의 다기능 특성이 미생물 감염에

대한 치료 접근법 개발에 대한 전망을 제공하면서 혁신적인 항균제, 항바이오필름제 및 항염증제의 잠재적 후보로 가치가 있음을 시사한다.

ABSTRACT

Multifunctional properties of symmetric tryptophan-rich antimicrobial peptides

Bobin Choi
Advisor: Prof. Sungtae Yang
Department of Biomedical sciences
Graduate School of Chosun University

Antimicrobial peptides (AMPs) are vital components of the innate immune system and play a critical role in safeguarding the host from microbial infections. Among these, symmetric tryptophan (Trp)-rich antimicrobial peptides (STRAMPs) are notable for their symmetrical structure and high Trp residue content. Despite their compact size, STRAMPs exhibit strong and broad-spectrum antimicrobial properties. In this study, I explored three distinct STRAMPs with unique structural features, focusing on their antimicrobial, antibiofilm, and anti-inflammatory capabilities. These STRAMPs demonstrated robust antibacterial effects against a range of microorganisms, including methicillin-resistant *Staphylococcus aureus* (MRSA) and multidrug-resistant *Pseudomonas aeruginosa* (MDRPA). Furthermore, they effectively hindered biofilm formation and eliminated pre-existing biofilms. Additionally, the STRAMPs exhibited anti-inflammatory characteristics by significantly reducing cytokine expression levels in lipopolysaccharide-stimulated macrophages. These findings suggest that the multifunctional properties of STRAMPs position them as potential candidates for innovative antimicrobial, antibiofilm, and anti-inflammatory agents, offering promising prospects for the development of therapeutic approaches against microbial infections.

1. Introduction

While conventional antibiotics have undeniably played a pivotal role in combating global epidemics because of their strong antimicrobial properties, the widespread abuse of these drugs have given rise to an abundance of drug-resistant bacteria, most notably multidrug-resistant strains [1]. This development presents an immense challenge to the field of clinical medicine. Currently, antibiotic resistance claims the lives of 700,000 individuals worldwide each year, and there is a profound concern that, in the absence of concerted efforts to curb resistance or develop innovative therapeutics, this grim statistic could skyrocket to a staggering 10 million deaths annually by 2050 [2]. Faced with the ominous threat that antibiotic resistance poses to human health, the discovery of new antibiotic classes has seen a marked decline [3]. However, recent research into antimicrobial peptides (AMPs), which are necessary parts of inborn host guard mechanisms, offers glimmer of hope in the ongoing battle against bacteria that are resistant to multidrug therapies, highlighting the potential advantages of AMPs [4].

AMPs have demonstrated their presence across a range of species, spanning from microbes and plants to mammals, where they play a crucial role in natural defense mechanisms [4]. These natural AMPs are typically characterized by their short length, consisting of fewer than fifty amino acids, and net positive charge ranges from +2 to +9 [5]. These attributes equip them with rapid bactericidal activity, diverse modes of action, and immunomodulatory effects [6]. In recent decades, extensive research has been dedicated to unraveling the structures and functions of AMPs, with the aim of shedding light on their systems of activity. These peptides typically possess distinct characteristics, marked by an abundance of amphipathic structures and basic amino acids that component groups of both hydrophilic and hydrophobic residues. While the precise intricacies of their mechanisms remain partially understood, a consensus has emerged that cationic AMPs engage in electrostatic interactions with the negatively charged membranes of bacteria. This interaction subsequently leads to cell death either by cell

membranes permeabiliztion through the formation of toroidal pores or barrel-stave or, alternatively, by employing a "carpet" mechanism to disrupt the membrane [7]. Additionally, it has been observed that in certain instances, these peptides repress macromolecular blend by gaining access to cytoplasm of the bacterial and binding to DNA or RNA, all without permeabilization of the membrane.

In contrast to conventional antibiotics, which primarily target explicit cellular components, AMPs achieve their bactericidal effects by physically disrupting bacterial membranes. This mechanism is less susceptible to the development of resistance through differential mutations. The physical disruption of bacterial membranes not only inhibits but can even reverse bacterial resistance, making AMPs a promising option in the ongoing battle against multidrug-resistant bacteria. Consequently, these peptides offer distinct advantages over conventional antibiotics as I strive to combat the escalating challenge of drug-resistant pathogens. Nevertheless, it is noteworthy that some AMPs have the capacity to lyse microbial cells as well as eukaryotic cells. Given therapeutic considerations, there is a compelling need to eliminate this activity against eukaryotic cells. Consequently, substantial consideration has been dedicated to the new AMP's development that heightened bacterial cell selectivity. It is important to acknowledge that natural AMPs have certain drawbacks, including relatively weaker antibacterial activity, limited stability, extended sequence lengths, and elevated synthesis costs.

Tryptophan-rich AMPs, represented by tritrpticin, have garnered considerable attention owing to their compact size and potent antibacterial properties. Tritrpticin is composed of mere 13 amino acids, featuring an abundance of cationic arginine (Arg) and hydrophobic tryptophan (Trp) residues. While the precise mechanism behind antibacterial activity of tritrpticin remains incompletely understood, it is widely recognized that the disruption of membranes facilitated by tritrpticin plays a pivotal role in its ability to eradicate bacteria. It is generally

hypothesized that the cationic Arg residues enable tritrpticin to interact with negatively charged surfaces and bacterial membranes through electrostatic attraction, while the Trp residues enable tritrpticin to embed itself within the lipid bilayer's nonpolar core in the bacterial membrane. An important feature is the favorable positioning of the indole side chains of Trp residues within of the lipid bilayer's interfacial region. These crucial attributes make tritrpticin highly effective toward Gram-positive, Gram-negative microbes, even when sequence of the peptide is remarkably short. As a result, tritrpticin has been considered as an encouraging foundation for the improvement of novel compounds to combat bacterial resistance.

Nonetheless, it is essential to recognize that tritrpticin exhibits significant hemolytic activity and toxicity towards mammalian cells, potentially limiting its therapeutic applicability. Addressing and mitigating these undesirable characteristics is a prerequisite before contemplating clinical applications. The structures of tritrpticin in a membrane-mimicking environment were elucidated using NMR techniques, revealing the β-turn conformation of tritrpticin. Previous investigations into the interplay between structure and function have revealed that the antibacterial effectiveness of tritrpticin is significantly influenced by its physicochemical and structural attributes, including charge, hydrophobicity, and secondary structure. Notably, analogs with symmetric amino acid sequences derived from the symmetric tritrpticin exhibited a considerable reduction in cytotoxic activity. Conversely, the replacement of proline (Pro) with alanine (Ala) in tritrpticin and indolicidin resulted in the reception of α-helical design, leading to the microbial viability's rapid eradication through efficient membrane depolarization. Proline induces a turn structure. Alanine induces the α-helix the best among amino acids. X (6-aminohexanoic acid) is responsible for removing peptide bonds and inducing hinge. It was synthesized by replacing the existing peptide, proline, with alanine and X. It was designed to find out how the action mechanism

and activity of peptides change when the turn structure is changed to α-helix and hinge.

This study focused on the synthesis of structurally varied symmetrical tritrpticins and examined their antibacterial, antibiofilm, and anti-inflammatory characteristics. A thorough exploration of the multifaceted properties exhibited by symmetrical tritrpticins holds the potential to open doors for the creation of innovative and efficacious treatments to address the escalating challenge of antimicrobial resistance.

2. Materials and Methods

2.1 Materials

The accompanying molecules were sourced by Sigma-Aldrich (Saint Louis, MO): calcium, N-phenyl-1-napthylamine, egg yolk L-phosphatidyl-DL-glycerol and egg yolk L-phosphatidylethanolamine, 3-(4,5-dimethylthiazol-2-yl)-2,5-diphenyl-2H-tetrazolium bromide (MTT). 3,3′-dipropylthiadicarbocyanine iodide (diSC_3-5) was given by Molecular Probes in Eugene, Oregon, United States of America). SYTOX Green was acquired from Life Technologies (Eugene, OR, United States of America).

2.2 Peptide synthesis

With N-(9-fluorenylmethoxy carbonyl) chemistry, I tested solid-phase synthesis to generate STP, STX, and STA peptides. The purification process involved the use of a suitable 0-90% H_2O/CH_3CN gradient and 0.05% trifluoroacetic acid on C_{18} column (250 mm × 20 mm; Vydac) during reversed-phase preparative HPLC. To assess hydrophobicity and purity (≥ 95%), analytical reversed-phase HPLC was conducted. Atomic masses of the unadulterated peptides were resolved with ESI-MS in Framingham, Massachusetts, United States of America (Fig. S1).

2.3 Circular dichroism (CD) spectroscopy

I conducted CD spectroscopic instrument with J-715 (Jasco, Japan) at 25ºC with 0.1 mm cuvette [8]. I dissolved the peptides in a solution consisting of 30 mM SDS micelles, 50% trifluoroethanol, and 10 mM $Na^+PO_4^{3-}$ buffer (pH 7.4). In the peptides, the α-helix's percentage was determined with the following formula:

$$\alpha\text{-helix } (\%) = -100 \times (\theta_{222} + 3000)/33000.$$

2.4 Antimicrobial assay

I assessed the peptide's antimicrobial activity in contrast to standard microorganisms, bacteria resistant to antibiotics, and yeast as per the rules laid out by the CLSI (Clinical and Laboratory Standards Institute) [9]. Gram-positive, gram-negative bacteria were sourced by the KCTC (Korean Collection for Type Cultures). To determine the peptide's minimum inhibitory concentration (MIC), I used a well-established technique. In summary, bacterial cells were mixed in 0.1% peptone to achieve a definitive concentration once they reached mid-log phase. Hence, in 0.1% peptone the peptides were sequentially mixed and combined with the bacteria in equal volume in 96 well plate. Each peptide's MIC was determined following 24 hours incubation period at 37 °C.

2.5 Time Killing kinetics assay

With MRSA (CCARM 3090) and MDRPA (CCARM 2095) strains, I assessed how quickly the peptides killed, as recently depicted. The initial culture density was around 1×10^6 CFU/ml. At time periods 0, 30, 60, 120, and 240 minutes, serial diluted by 50 μl 10 times of the bacteria was put onto Luria-Bertani (LB) agar plates. These plating was performed in both the presence of peptides and absence of peptides (control). After 1 day of incubation at 36.8 °C, I counted the colonies to assess the antimicrobial efficacy of the peptides.

2.6 Hemolytic activity

Sheep red blood cells were cleaned with PBS, followed by the preparation of 4% blood in PBS. A 96 well plate was then prepared, with each well containing 100 μl of various peptide concentrations. Subsequently, I added 100 μl of the 4% blood to each well. The plate was grown for 1 hour at 36.8°C, after which it was centrifuged, and the absorbance at 450 nm in the supernatant was estimated. As a positive control, 1% Triton X-100 was used, while PBS served as the negative control.

2.7 Cytotoxicity assay

Peptide's cytotoxicity against mouse macrophage cell RAW264.7 was evaluated using the MTT assay [10]. At 36.8°C, in a humidified air with 5% CO_2, RAW264.7 cells were grown in DMEM with 10% FBS. The cells were grown overnight in 96 well plates in DMEM. Following this incubation, MTT was injected to each well in the 96 well plate and grown for 3 hours at 36.8°C. After removing the supernatant, to dissolve the formazan crystals formed, 100 µL of DMSO was added, and the optical density (OD) was evaluated at 550 nm with a plate reader (Bio-Tek Instruments EL800, United States of America).

2.8 Outer membrane (OM) permeabilization assay

I used the NPN (1-N-phenylnaphthylamine) fluorescent dye test to evaluate the peptides' ability to the outer membrane permeabilization [11]. In brief, I harvested *E. coli* (KCTC 1682) cells and diluted to a 600 nm optical density of 5 mM 0.2 glucose in 5 mM HEPES buffer (pH 7.4). Subsequently, the cell suspension was grown with 10 µM NPN. In 1 cm cuvette, different concentrations of the peptides were then added to 3 ml of the cell culture. Fluorescence measurements were conducted with a fluorescence spectrophotometer. It was conducted at an emission wavelength of 420 nm and an excitation wavelength of 350 nm.

2.9 Inner membrane (IM) permeabilization assay

I assessed the peptides' capacity to saturate the inner membrane by measuring cytoplasmic activity of *β*-galactosidase in *E. coli* with ONPG (*o*-nitrophenyl-*β*-galactoside) [12]. *E. coli* cells were diluted to 600 nm optical density of 0.05 after being washed 3 times in 10 mM PBS (pH 7.4) with 1.5 mM ONPG. In each well of sterile 96 well plate, 150 μl of the bacteria was combined with 50 μl of PBS with the peptide at various concentrations. The rate of inner membrane permeability was evaluated by monitoring the absorbance at 405 nm during the hydrolysis of ONPG to *o*-nitrophenol.

2.10 Bacterial membrane depolarization assay

I used diSC_3-5, the membrane potential-sensitive fluorescent dye, to assess the peptides' ability to induce cytoplasmic membrane depolarization [13]. I harvested *S. aureus* (KCTC 1621) cells and diluted to 600 nm optical density of 0.05 in 5 mM HEPES buffer with pH 7.4 and 20 mM glucose. After incubating with 0.4 mM diSC_3-5 and 100 mM K^+, the fluorescence of the cell suspension remained stable. Fluorescence measurements were carried out with a RF-5300PC (Shimadzu, Kyoto, Japan). It was conducted at an emission wavelength of 670 nm and an excitation wavelength of 622 nm. The peptides were introduced into a 1 cm quartz cuvette containing 3 ml of the cell solution at their 2× MIC. Fluorescence changes were estimated over a duration of 500 seconds.

2.11 SYTOX Green (SyGr)uptake assay

I utilized the SyGr assay to assess peptide's membrane permeabilization caused in *S. aureus* (KCTC 1621) [14]. In brief, suspensions of *S. aureus* (KCTC 1621) in 5 mM HEPES, 20 mM glucose, 10 mM KCl, and pH 7.4 were set up. These suspensions were incubated in the unlit for 15 minutes at 37°C. The SyGr uptake assay was conducted with the RF-5300PC (Shimadzu, Kyoto, Japan). It was conducted at an emission wavelength of 520 nm and an excitation wavelength of 485 nm after adding the peptides to a final concentration equivalent to 2× MIC.

2.12 Flow cytometry

I evaluated the integrity of the bacteria membranes through flow cytometry, assessing propidium iodide (PI) uptake [15]. The 600 nm absorbance of MRSA and MDRPA was diluted until it was around 0.4. Subsequently, with 10 mM PBS (pH 7.4), the bacteria were diluted 10 times. The peptide, at a concentration of 2× MIC, was introduced, and for 30 minutes the solution was incubated at 36.8°C. After incubation, PI was added to achieve a last concentration of 10 μg/ml and then incubated for an extra 30 minutes. FACScan machine was used to measure PI fluorescence at the end.

2.13 Calcein dye leakage assay

I optimized the preparation of calcein entrapped large unilamellar vesicles (LUVs) [16]. Initially, negatively charged lipids PE/PG (5:5, w/w) were liquefied in chloroform, dried using a nitrogen, and then rehydrated in a dye buffer solution (at pH 7.4, comprising 0.1 mM EDTA, 10 mM Tris, 70 mM calcein, and 150 mM NaCl). This liquid was frozen and melted 20 times freeze-thaw in liquid nitrogen and was subsequently ejected after 21 cycles with LiposoFast with filters featuring 100 nm sizes. To eliminate untrapped calcein, gel was used. Calcein leakage from the liposomes was assessed at ambient temperature with a RF-5300PC. It was conducted with an emission wavelength of 520 nm and an excitation wavelength of 490 nm. Dye release was achieved with 0.1% Triton X-100.

2.14 Biofilm Eradication assay (MBEC)

I investigated the efficacy of the peptides with MRSA (CCARM 3090) and MDRPA (CCARM 2095) biofilms [17, 18]. In 96 well culture plates, 200 μl of the bacteria cultures in 0.2% glucose Mueller-Hinton broth (MHB) supplemented were grown for 1 day at 36.8°C. This incubation was conducted both in the presence of peptides (serial diluted from 128 μM to 1 μM) and in their absence. Each condition was assessed in triplicate. Following the incubation period, the liquid was gently aspirated, and to remove unattached bacteria, 250 μl of PBS solution was washed three times. The wells were then air-dried and fixed by adding 200 μl of 98% methanol to each well during 15 minutes. After dried the plates, 100 μl of 0.1% crystal violet were stained to the wells for 5 minutes. Supernatant stain was washed away carefully with water before the plates were dried. The stain was solubilized again by adding 100 μl of 95% ethanol and shaking for 30 minutes on a shaker. Finally, at 600 nm, the absorbance was estimated.

2.15 Confocal laser-scanning microscopy (CLSM)

MRSA and MDRPA (1×10^6 CFU/mL) were grown in MHB-glucose media in 12 well plates for 1 day containing discs to culture biofilm. With 1X PBS,

cells were washed three times before being transferred to fresh 12 well plates containing STP, STX, and STA (MBEC: 16 μM). They were then incubated for an additional 24 hours. Following incubation, the discs were removed, with 1X PBS washed twice, and stained with 40 μM propidium iodide and 6.7 μM SYTO 9. Images of the biofilm on the discs were acquired with CLSM and analyzed with ZEN 2009 (ZEISS, Jena, Germany) at 36.8°C, in the dark, after 30 minutes incubation.

2.16 Measurement of tumor necrosis factor-α (TNF-α), interleukin 6 (IL-6) release from LPS-stimulated RAW264.7 cells

I investigated the peptide induced inhibition of proinflammatory cytokines in LPS-stimulated macrophage cells, specifically tumor necrosis factor (TNF)-α and interleukin (IL)-6. Mouse macrophage cell RAW 264.7 (2×10^6 cells/mL) were plated to 96 well plate (100 μL/well). LPS was stimulated from *E. coli* (20 ng/mL) for 1 day in the existence of the peptide and absence of the peptide. After 1 day of incubation, supernatant of the culture was collected for ELISA (Enzyme-Linked Immunosorbent Assay) to quantify the levels of the inflammatory cytokines TNF-α and IL-6. The nitrite level was determined with Griess reagent (2% phosphoric acid, 0.1% naphthylethylenediamine dihydrochloride, and 1% sulfanilamide). The release of TNF-α and IL-6 were measured with the manufacturer's instructions with the DuoSet ELISA kit (R&D Systems, Minneapolis, United States of America).

2.17 Reverse-transcription polymerase chain reaction (RT-PCR)

I followed a previously established RT-PCR protocol [19]. In the presence of the peptide and absence of the peptide RAW264.7 cells were grown into 6 well plates at a density of 5×10^5 cells per well and stimulated with *E. coli*. After 4 hours incubation (for TNF-α and IL-6), RNA was extracted with TRIzol, and the RNA concentration was quantified with a Nanodrop spectrophotometer. cDNA synthesis was performed with Oligo-$d(T)_{15}$ primers and the Reverse Transcriptase kit, following the manufacturer's instructions, starting with 2 μg of total RNA. The

resulting cDNA products were amplified with the following primers: TNF-α (forward 5´-CCTGTAGCCCACGTCGTAGC-3´, reverse 5´-TTGACCTCAGCGCTGAGTTG-3´), IL-6 (forward 5´-ACAACCACGGCCTTCCCTACT -3´, reverse 5´-CACGATTTCCCAGAGAACATG-3´), and GAPDH (forward 5´-GACATCAAGAAGGTGGTGAA-3´, reverse 5´-TGTCATACCAGGAAATGAGC-3´). The PCR amplification consisted of an initial denaturation step at 94°C for 3 minutes, followed by 28 cycles of denaturation at 94°C for 1 minute, annealing at 60°C for 1 minute, and extension at 72°C for 1 minute, with a final extension at 72°C for 3 minutes. Electrophoresis was employed to separate the PCR products, which were subsequently visualized under UV light.

3. Results

3.1 Peptide design and synthesis

Proline residues are recognized for their significant roles in the formation and architecture of membrane proteins. Schibli and colleagues revealed that tritrpticin adopts a random coil conformation when placed in Tris buffer. However, in SDS micelles, it takes on a configuration featuring two consecutive turns, centered around the two Proline residues. This distinctive structure, influenced by the presence of these two Proline residues, generates a stable amphipathic turn configuration, where Tryptophan residues are sequestered within the micelle, while Arginine residues are situated on the opposite side of this structure. To enhance our comprehension of its bacterial cell selectivity and to establish a foundation for comprehending its multifaceted properties, we formulated and synthesized three symmetrical TRAMPs by substituting the two Proline residues with Alanine or 6-aminohexanoic acids. The sequences employed in this research are shown in Table 1.

3.2 Secondary structure of peptides

To additionally analyze the peptide's secondary structure in various conditions, I conducted Circular Dichroism (CD) Spectroscopy in both aqueous conditions (10 mM PBS) and environments mimicking membranes of the bacteria (30 mM sodium dodecyl sulfate micelles, 50% TFE). As depicted in Figure 1, STP, STX, and STA exhibited negative peaks at 220, 225, 223 nm, separately, along with positive peaks at 195, 210, and 192 nm. These characteristic spectral features indicate the presence of a stable rigid turn, flexible turn, and α-helical conformation in the peptides.

3.3 Antimicrobial activity

I assessed peptide's antimicrobial activity against Gram-positive organisms, resistant Gram-positive organisms, Gram-negative organisms, resistant Gram-negative organisms, and yeast. With the microdilution strategy, I determined the

minimum inhibitory concentrations (MICs) of STP, STX, STA, and the control peptide melittin for comparison. STP exhibited inhibitory effects at a concentration of 16 μM against *S. aureus*, MRSA, VREF, *S. typhimurium*, and MDRPA (Table 2). It also exhibited inhibitory effects at a concentration of 32 μM with *P. aeruginosa, B. subtilis, S. epidermidis*, and *E. coli*. STX displayed inhibitory effects at a concentration of 16 μM against *B. subtilis*, MRSA, VREF, and MDRPA. Additionally, it exhibited inhibitory effects at a concentration of 32 μM against *S. aureus, P. aeruginosa*, and *S. typhimurium*. Furthermore, STX displayed inhibitory effects at a higher concentration of 64 μM with *S. epidermidis* and *E. coli*. STA showed inhibitory activity at 8 μM in *S. typhimurium* and at 16 μM in *S. aureus, B. subtilis*, MRSA, VREF, *E. coli*, and MDRPA. Additionally, STA exhibited inhibitory activity at concentration of 32 μM in *S. epidermidis* and *P. aeruginosa*. These discoveries feature the capability of these peptides as effective antibacterial specialists, especially against the tested resistant pathogens.

3.4 Time-killing kinetic assay

I conducted a time-killing kinetic assay to determine the time it took for MRSA and MDRPA exposed to peptides at their MICs (16 μM) to be killed. I used melittin as a control peptide. The results showed that STP, STX, and STA peptides, like melittin, completely killed MRSA and MDRPA within 30 minutes (Figure 2).

3.5 Hemolytic activity

I measured the peptide's hemolytic activity with sheep red blood cells (sRBCs) to assess peptide's potential cytotoxic effects on mammalian cells (Figure 3). STP exhibited no hemolysis or less than 40% hemolysis at 128 μM, while at 256 μM, it showed 60% hemolytic activity. STX peptide displayed no hemolytic activity at 256 μM. Similarly, STA showed no hemolysis or less than 20% hemolysis at 128 μM, and at 256 μM, it exhibited less than 50% hemolysis.

3.6 Cytotoxicity against RAW 264.7 macrophage cells

Lipopolysaccharides (LPS) are gram-negative bacteria's very important outer membrane parts. These huge amphipathic glycoconjugates normally comprise of a lipid space (hydrophobic), giving rise to their classification as lipoglycans because of the existence of lipid and sugar molecules. To assess the cytotoxic effects of STP, STX, and STA on RAW264.7 cells, I conducted MTT assay (Figure 4). RAW264.7 cells were exposed to peptides at different concentrations from 1 μM to 128 μM. STP displayed over 60% cell viability at 16 μM but exhibited only 15% cell viability at 32 μM, with no cell viability observed at 64 μM and 128 μM. STX showed more than 60% cell viability at 32 μM and maintained more than 20% cell viability at 64 μM. STA demonstrated the lowest cytotoxicity, as it maintained more than 60% cell viability even at 64 μM.

3.7 Outer membrane permeability, and Inner membrane permeability

I conducted several fluorophore-based studies to assess the impact of STP, STX, and STA on the membrane permeability of *S. aureus* including assessing outer membrane permeability with NPN and inner membrane permeability with ONPG. Exceptionally membrane dynamic peptides can disrupt the membrane of bacteria, leading to a fast arrival of dyes and an increase in fluorescence intensity. NPN, a hydrophobic fluorescent test, is typically extinguished in watery conditions, however, fluoresces strongly in hydrophobic conditions. Under typical circumstances, NPN cannot penetrate the outer membrane of bacteria. However, when the outer membrane is permeabilized, NPN can go into the hydrophobic membrane conditions, resulting in increased fluorescence within the cell. The NPN's expanded fluorescence indicates a weakening or loss of integrity in the outer membrane bacteria's construction. Melittin was effective at permeating the *E. coli* outer membrane, depending on the dose (Figure 5). Similarly, STP, STX, and STA demonstrated a high level of outer membrane permeabilization, resembling the behavior of melittin. In addition to outer membrane permeabilization, the translocation of peptides into the inner membrane is a critical step in membrane disruption. I used the lactose-permeable strain *E. coli* ML-35 to evaluate the

peptide's ability to penetrate the inner membrane. STP rapidly increased inner membrane permeability, reaching 80% ONPG permeability at 180 minutes (Figure 5). However, the control peptide melittin, as well as STX and STA, reduced inner membrane permeabilization, resembling the behavior of buforin-2. These results suggest that STP and STX strongly damaged the cell's inner membrane, whereas STA did not have the same effect.

3.8 Cytoplasmic membrane depolarization

To evaluate the mitochondrial *S. aureus*' membrane potential, I employed diSC_3-5, a commonly used fluorescent test. Over a 500 seconds period, I observed the peptide-induced depolarization, as illustrated in Figure 6. All peptides incited cytoplasmic layer depolarization at 1 × MIC. In particular, the membrane-targeting AMP melittin, as well as STP, STX, and STA, totally cytoplasmic membrane was depolarized at 1 × MIC. In contrast, intracellular targeting buforin-2 didn't cause membrane depolarization.

3.9 SYTOX Green (SyGr) uptake assay

To gain deeper insights into the peptide's action mechanism, I conducted the SyGr uptake assay on *S. aureus* (KCTC 1621). SyGr, which has a high affinity for DNA binding, can evaluate the S. aureus membrane permeability with the peptides. (Figure 7). As contrasted to melittin, STP, STX, and STA did not exhibit remarkable SyGr influx, like buforin2 at 1 × MIC. These findings suggest that the peptides may not cause substantial disruption to the bacterial membrane, distinguishing their mechanism of action from that of melittin.

3.10 Flow cytometry analysis

I conducted flow cytometry to assess the membrane integrity of resistant gram-positive and gram-negative bacteria by staining them with propidium iodide (PI). The bacterial cells stayed in same shape in the peptide's absence, but in the peptide's presence, the cell membranes were visibly damaged (Figure 8, Figure 9).

STP showed a further significant membrane-disrupting effect against Gram-positive (G(+)) MRSA (76.49%) than Gram-negative (G(-)) MDRPA (49.34%), highlighting its solid membrane focusing on ability against G(+) bacteria. STX exhibited a similar membrane focusing on capacity against both MRSA (64.9%) and MDRPA (43.55%). Conversely, STA displayed a further strong membrane-disastrous effect against MRSA (90.49%) than MDRPA (32.21%). These outcomes highlight the membrane target properties of the STRAMP peptides, which can disrupt bacterial cell membranes' integrity. This feature contributes to antimicrobial action against resistant bacteria. Consequently, these peptides hold promise as potential possibility for fighting antibiotic-resistant pathogens, because of their distinct effects on both G(+) and G(-) bacteria.

3.11 Calcein dye leakage

I conducted a fluorescent leakage assay to investigate whether STP, STX, and STA could disrupt liposome membranes (Figure 10). I used phosphatidylethanolamine (PE) and phosphatidylglycerol (PG) to mimic bacterial cell membranes. All peptides were tested for their ability to induce calcein leakage from PE:PG (1:1, w/w) large unilamellar vesicles (LUVs). STX, STA, and the control peptide Melittin rapidly and significantly induced calcein leakage in LUVs. In contrast, STP exhibited a slower disruption of the liposomes. These results suggest that STP, STX, and STA disrupt liposomes by creating pores in the membrane.

3.12 Biofilm inhibition and eradication activity

The formation of bacterial biofilms is recognized as a significant threat that contributes to disease progression and antibiotic resistance. Methicillin-resistant *Staphylococcus aureus* (MRSA) (CCARM 3090) is a testing bacterial infection to treat because of its antibiotic resistance, and *Pseudomonas aeruginosa* (MDRPA) (CCARM 2095) is a significant pathogen known for its biofilm formation. I assessed the ability of STP, STX, and STA to inhibit biofilm growth and eradicate

mature biofilms of MRSA (Figure 11) and MDRPA (Figure 13) strains. At 16 μM, identical to 1 × MIC, all peptides exhibited potent biofilm inhibition and eradication effects against both MRSA and MDRPA strains. Notably, STP demonstrated 90% MBIC (minimal biofilm inhibition concentration) and 90% MBEC (minimal biofilm eradication concentration) at 16 μM, respectively. Interestingly, the control peptide LL-37 did not exhibit significant activity, even at 50% concentration. I further confirmed the eradication of biofilm visually using confocal laser scanning microscopy (CLSM) and a viability staining kit (Figure 12 and Figure 14).

3.13 Anti-inflammatory activity

In response to stimuli such as LPS, humans produce the cytokines tumor necrosis factor (TNF)-α and interleukin (IL)-6, which are major inflammatory substances generated during bacterial infections. As demonstrated in Figure 15, STP, STX, and STA effectively controlled the LPS-induced inflammatory response in cells at 8 μM, 16 μM, and 32 μM concentrations. Contrastably, LL-37 exhibited less inhibitory activity. Specifically, STP achieved over 60% inhibition of LPS-induced IL-6 production at a concentration of 8 μM.

3.14 Reverse-transcription polymerase chain reaction (RT-PCR)

I conducted RT-PCR to investigate the expression of TNF-α and IL-6 mRNA in lipopolysaccharide (LPS)-stimulated cells, aiming to assess presence of peptides influenced the production of inflammatory cytokines. All peptides were administered at 16 μM. While STP, STX, and STA displayed faint bands like control and control peptide LL-37, a distinct band was observed in the case of TNF-α with LPS treatment (Figure 16). Furthermore, STP, STX, and STA effectively or moderately inhibited IL-6 expression. The peptides' ability to inhibit cytokine expression followed this order: STP > STA > STX.

4. Discussion

The rise of antibiotic resistance poses an increasingly serious global public health challenge. Amidst this issue, attention is turning to antimicrobial peptides (AMPs) as a novel kind of antibiotic to combat infectious diseases induced by drug-resistant bacteria. Among these AMPs, TRAMPs stand out due to their distinctive amino acid makeup, which grants them potent and wide-ranging antibacterial properties even with relatively short peptide lengths. This quality makes them an appealing candidate for therapeutic development. Notably, TRAMPs like tritrpticin and indolicidin have demonstrated their effectiveness with both Gram-positive and Gram-negative bacteria, counting those that have created reistance from conventional antibiotics. Nevertheless, there are some hurdles to overcome, such as TRAMP's limited selectivity for bacterial cells and their potential harm to mammalian cells, which can impede their therapeutic use. In our previous research, I addressed these challenges by designing symmetric TRAMPs inspired by symmetric tritrpticin and indolicidin, showing improvements in antibacterial selectivity. I observed that symmetric α-helical TRAMPs, when compared to their parent peptides, maintained their ability to combat Gram-negative bacteria, exhibited enhanced effectiveness against Gram-positive bacteria, and experienced a notable reduction in their harm to mammalian cells.

STP was found to be a rigid-turn structure in CD experiments. STP demonstrated inhibitory responses at 16 μM concentration when exposed to *S. aureus*, MRSA, VREF, *S. typhimurium*, and MDRPA. Furthermore, it displayed inhibitory effects at 32 μM concentration when tested with *P. aeruginosa*, *B. subtilis*, *S. epidermidis*, and *E. coli*. Time-killing kinetic assay showed that MRSA, MDRPA bacteria were killed the fastest compared to other peptides. Outer membrane permeabilization assay showed the lowest permeability at 10 μM concentrations, but the graph rose sharply at 20 μM. Inner membrane permeabilization assay showed 40% permeation at 0 minutes and 80% at 180 minutes. The depolarization experiment showed that STP disrupted the membrane

of *S. aureus* highest fluorescence. However, in SYTOX, graphs appeared along the baseline. These results represent STP only targets the outer membrane and does not show any effect on the inner membrane in Gram-positive bacteria. To make this result more clearly, I performed flow cytometry analysis, and it was shifted 76% in MRSA and 49% in MDRPA. Anti-inflammatory activities were conducted to find out the inflammatory response to animal cells. At all concentrations showed lower inflammation than 10% in TNF-α, and in IL-6, inflammation was reduced from 70% to 20% when the peptide concentration was raised from 8 μM to 16 μM. RT-PCR experiments were conducted to confirm this result, and neither TNF-α nor IL-6 showed bands, so STP inhibits inflammation. RT-PCR experiments were conducted out to validate these results, and in both cases, TNF-α and IL-6 did not produce detectable bands, thus affirming that STP effectively suppresses inflammation.

CD spectra showed that STX is a flexible turn structure. STX indicated antimicrobial inhibitory activity at 16 μM in *B. subtilis*, MRSA, VREF, and MDRPA. Furthermore, it demonstrated inhibitory effects at 32 μM against *S. aureus*, *P. aeruginosa*, and *S. typhimurium*. In addition, STX exhibited inhibitory effects at a higher concentration of 64 μM when exposed to *S. epidermidis and E. coli*. In the time-killing kinetic assay, STX exhibited a slower rate of eradication against MRSA and MDRPA when compared to the other two peptides. STX showed the lowest cytotoxicity in RAW267.4 cells and demonstrated minimal hemolytic activity in sheep red blood cells. During the outer membrane permeabilization assay, even at a low 2 μM concentration, it exhibited higher permeability compared to the control peptide melittin. In the inner membrane permeabilization assay, over 60% permeability was observed at both 0 minute and 180 minutes. In membrane depolarization experiment with *S. aureus*, STX displayed noticeable effects. However, in the SYTOX assay, the graph remained consistent with the baseline, indicating that STX selectively targets the outer membrane without affecting the inner membrane in G(+) bacteria. STX shifted the

least (64% in MRSA and 43% in MDRPA) in flow cytometry analysis. The biofilm inhibition assay showed 90% biofilm inhibition at 16 μM, and the biofilm eradication assay showed 90% eradication at 32 μM in the MRSA strain. The biofilm inhibition and eradication assay were effective at 16 μM in the MDRPA strain. STX demonstrated a minimal inflammatory response to TNF-α. However, in the case of IL-6, an initial inflammatory response exceeding 80% was observed at 8 μM. This response subsequently decreased to 40% at 16 μM, and further reduced to 10% at 32 μM. Notably, the higher the concentration, the more effective the suppression of the inflammatory response. Both TNF-α and IL-6 exhibited observable bands in the RT-PCR analysis.

CD experiments revealed that STA exhibited α-helical structure. At concentrations of 8 μM, STA demonstrated inhibitory effects against *S. typhimurium*. At 16 μM, it displayed inhibition against *B. subtilis*, *S. aureus*, MRSA, VREF, *E. coli*, and MDRPA. Furthermore, STA exhibited inhibitory activity at 32 μM against *S. epidermidis* and *P. aeruginosa*. These results underscore the promising potential of these peptides as potent antibacterial agents, especially in combating the tested drug-resistant pathogens. Time-killing kinetic assay showed that MRSA, MDRPA bacteria were killed the fastest compared to other peptides. As a result of the experiment, it was confirmed that the number of cells of MRSA and MDRPA decreased significantly within 30 minutes, killing drug-resistant positive bacteria and drug-resistant negative bacteria in very short time. Time-killing kinetic assay confirmed huge decrease in the quantity of MRSA and MDRPA cells within 30 minutes, effectively eradicating both drug-resistant positive and drug-resistant negative bacteria immediately. Compared to other peptides, STA exhibited the lowest hemolytic activity in sheep red blood cells, with under 10% hemolysis observed at 120 μM concentration. Cell viability exceeded 90% at 16 μM and remained above 80% at 32 μM in RAW267.4 cells. While STA successfully penetrated the outer membrane of *E. coli*, the extent of penetration through the inner membrane was less than that achieved by the control peptide,

buforin-2. The membrane of S. aureus experienced depolarization, but the SYTOX experiment kept the graph at a steady baseline without any notable increase. Thus these results indicated STA specifically targets the outer membrane in Gram-positive bacteria. Similar results were observed in flow cytometry analysis, showing 90% shift in MRSA, a drug-resistant G(+) bacterium, and 32% shift in MDRPA, a drug-resistant G(-) bacterium. In the calcein dye leakage assay with large unilamellar particles prepared at 1:1 PE:PG ratio to mimic the bacterial membrane, it was observed that STA exhibited the most significant membrane depolarization compared to other peptides. At 1 μM concentration, STA successfully suppressed 50% of biofilms, and at 16 μM, it demonstrated an impressive 90% inhibition of biofilm formation in MRSA bacteria. However, 90% of biofilms were eradicated at 16 μM concentration. The biofilm experimental results for MDRPA bacteria differ from those of MRSA. At concentration of 16 μM, STA exhibited a 90% minimal biofilm inhibition rate, along with 70% minimal biofilm eradication concentration at 8 μM and 90% MBEC at 16 μM. STA demonstrated a minimal inflammatory response to TNF-α. However, in the case of IL-6, inflammatory response exceeding 60% was observed at 8 μM and this response subsequently decreased to 20% at 16 μM, and further reduced to 10% at 32 μM. Notably, the higher the concentration, the more effective the suppression of the inflammatory response. The band was visible on TNF-α but not on IL-6 in the RT-PCR analysis.

Table1. Amino acid sequence and physicochemical properties of STP, STX, STA

Peptides	Amino acid sequence [a]	Net charge	t_R (min)[b]	MS Analysis		
				z	m/z calculated	m/z found[c]
STP	RRF**P**WWW**P**FRR-NH_2	+4	29.475	$[M+2H]^{2+}$	845	845.5
STX[d]	RRF**X**WWW**X**FRR-NH_2	+4	30.185	$[M+2H]^{2+}$	861.02	861.54
STA	RRF**A**WWW**A**FRR-NH_2	+4	29.232	$[M+2H]^{2+}$	818.94	819.46

[a] Bold and underlined characters are the amino acid residues that were substituted in this study.
[b] Retention time of (Rt) was measured by analytical RP-HPLC with C_{18} column (5 mm; 4.6 mm × 250 mm; Vydac).
[c] Molecular mass was determined using matrix-assisted laser desorption/ionization (MALDI)-time-of-flight (TOF)-mass spectrometry (MS)
[d] X is 6-aminohexanoic acid

Table2. Antimicrobial activity of STP, STX, STA against pram-positive and gram-negative bacterial standard strains

Microorganism	Minimal inhibitory concentration (MIC)[a] (μM)			
	STP	STX	STA	Melittin
Gram-positive organisms				
S. aureus (KCTC 1621)	16	32	16	4
S. epidermidis (KCTC 1917)	32	64	32	16
B. subtilis (KCTC 3068)	32	16	16	8
Resistant Gram-positive organisms				
MRSA[b] (CCARM 3090)	16	16	16	4
VREF[c] (ATCC 51559)	16	16	16	16
Gram-negative organisms				
E. coli (KCTC 1682)	32	64	16	8
P. aeruginosa (KCTC 1637)	32	32	32	32
S. typhimurium (KCTC 1926)	16	32	8	8
Resistant Gram-negative organisms				
MDRPA[d] (CCARM 2095)	16	16	16	4
Yeast				
C.albicans (KCTC 7965)	64	16	32	4
C.albicans (KCTC 7121)	32	32	16	4

[a] MIC was determined as the lowest concentration of peptide that caused 100 % inhibition of microbial growth.

[b] *MRSA*: methicillin-resistant *Staphylococcus aureus.*

[c] *VREF*: vancomycin-resistant *Enterococcus faecium.*

[d] *MDRPA*: multidrug-resistant *Pseudomonas aeruginosa.*

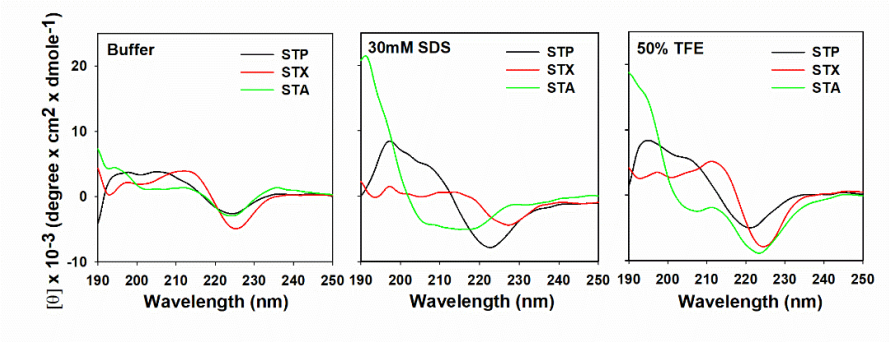

Figure 1. The CD (circular dichroism) spectra of STP, STX and STA in aqueous buffer and membrane-mimicking environments: 10 mM sodium phosphate buffer (pH 7.4), 30 mM SDS, 50% TFE. The mean residue ellipticity was plotted against wavelength. The values from three scans were averaged per sample.

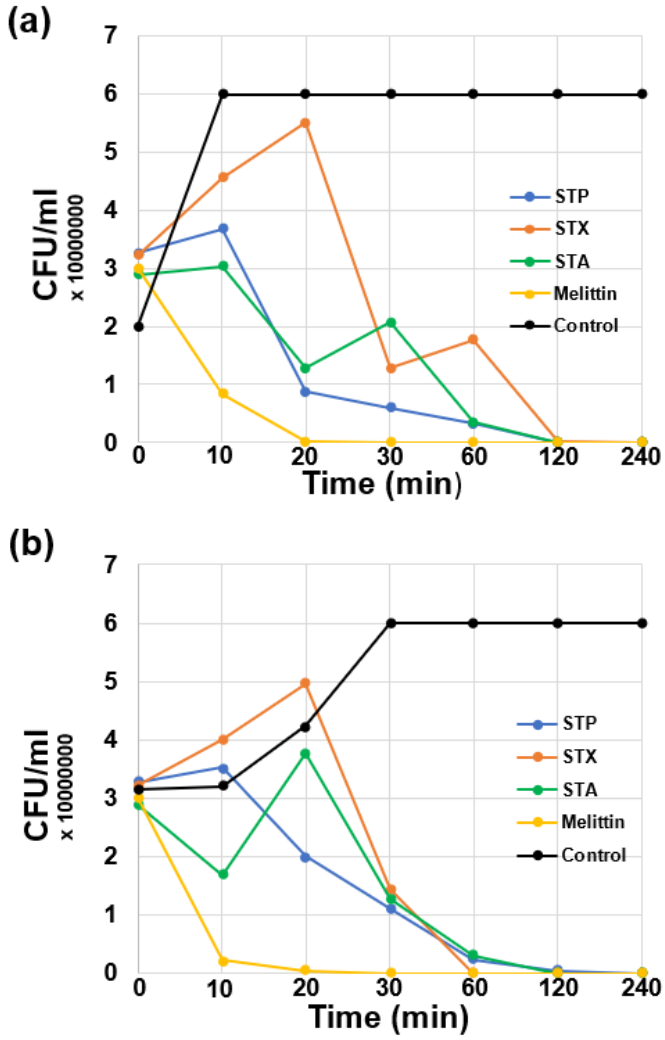

Figure 2. Time-kill curves of STP, STX, and STA with control peptide melittin against (a) methicillin-resistant *Staphylococcus aureus* (MRSA) (CCARM 3090), (b) multidrug-resistant *Pseudomonas aeruginosa* (MDRPA) (CCARM 2095) at 1 × MIC. The dotted line indicates 50% reduction from initial OD.

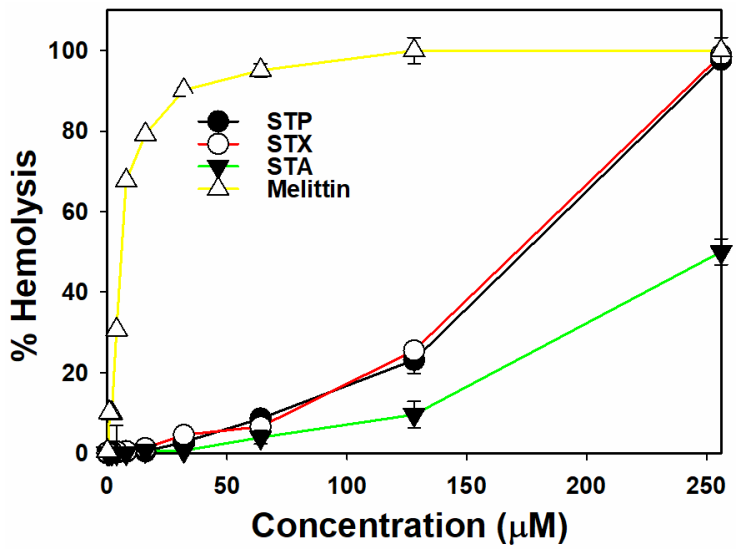

Figure 3. Hemolytic activity of STP, STX and STA, measured as percentage hemolysis in sheep red blood cells (sRBCs).

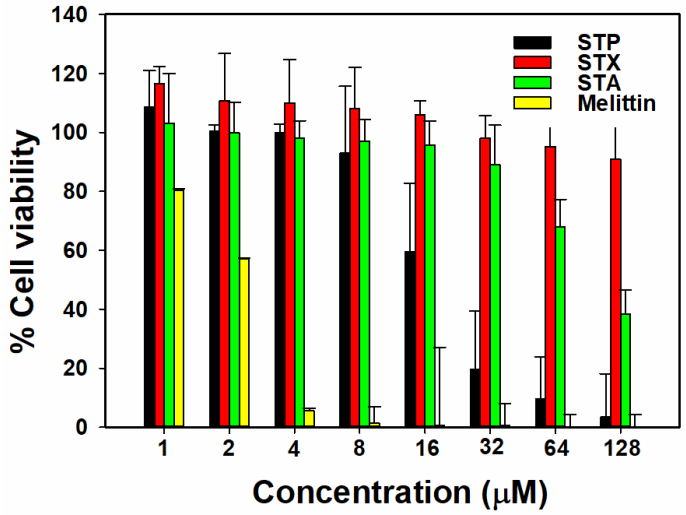

Figure 4. Cytotoxicity of STP, STX and STA against mouse macrophage RAW264.7 cells.

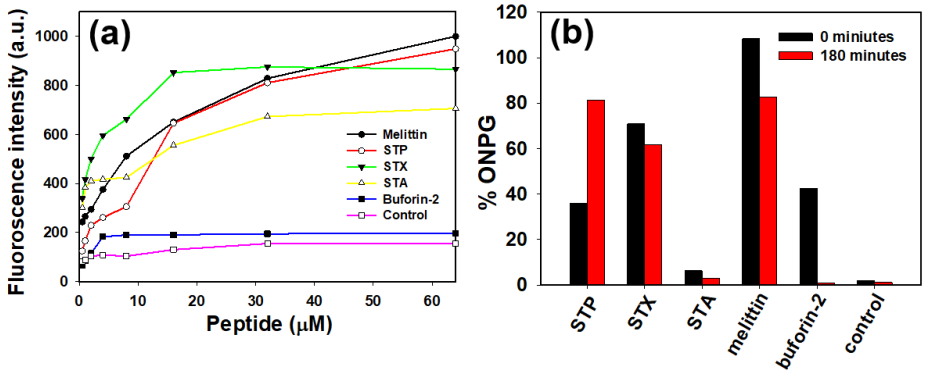

Figure 5. (a) The outer membrane permeability of the peptides. Membrane uptake of 1-N-phenylnaphthylamine (NPN) of *E. coli* (KCTC 1682) in the presence of different concentrations of the peptides. Inner membrane permeability of the peptides. (b) Hydrolysis of *ortho* nitrophenyl-*β*-galactoside (ONPG) due to release of cytoplasmic *β*-galactosidase of *E. coli* ML-35 cells treated with peptides at different concentration was measured spectroscopically at the absorbance of 405 nm as a function of time.

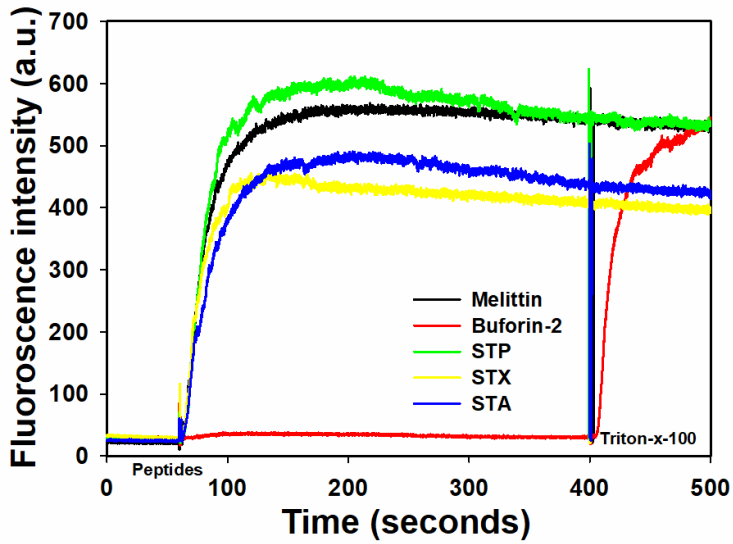

Figure 6. Cytoplasmic membrane depolarization of *S. aureus* (KCTC 1621) treated with STP, STX, and STA (2 × MIC), as assessed by the release of the membrane potential-sensitive dye diSC_3-5.

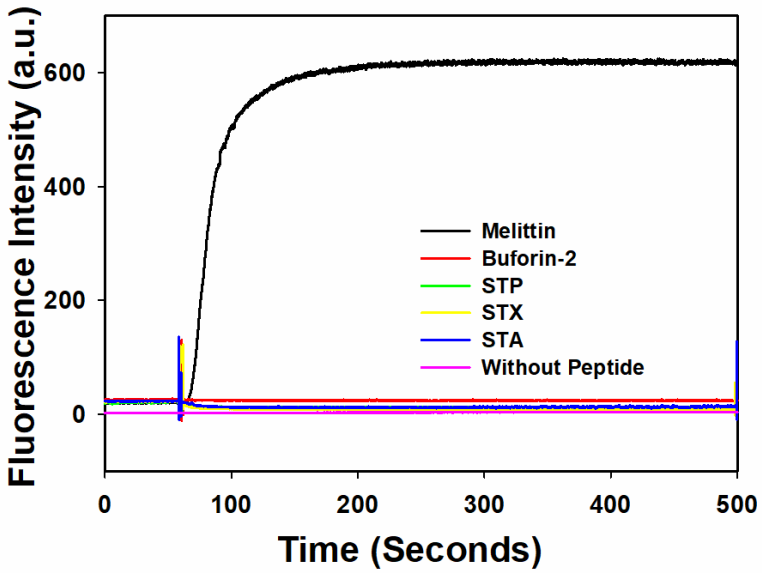

Figure 7. SYTOX Green uptake of *S. aureus* (KCTC 1621) treated with STP, STX, and STA (2 × MIC).

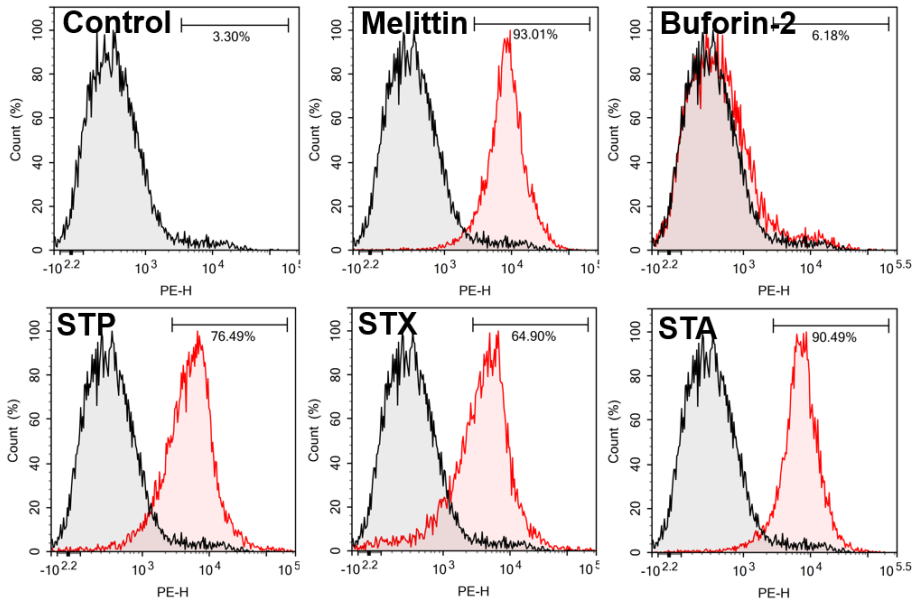

Figure 8. Interaction of STP, STX and STA with membranes. Membrane integrity disruption of MRSA (CCARM 3090) in presence of peptides (1 × MIC), measured by an increase in fluorescent intensity of propidium iodide (PI). The control was processed without peptides.

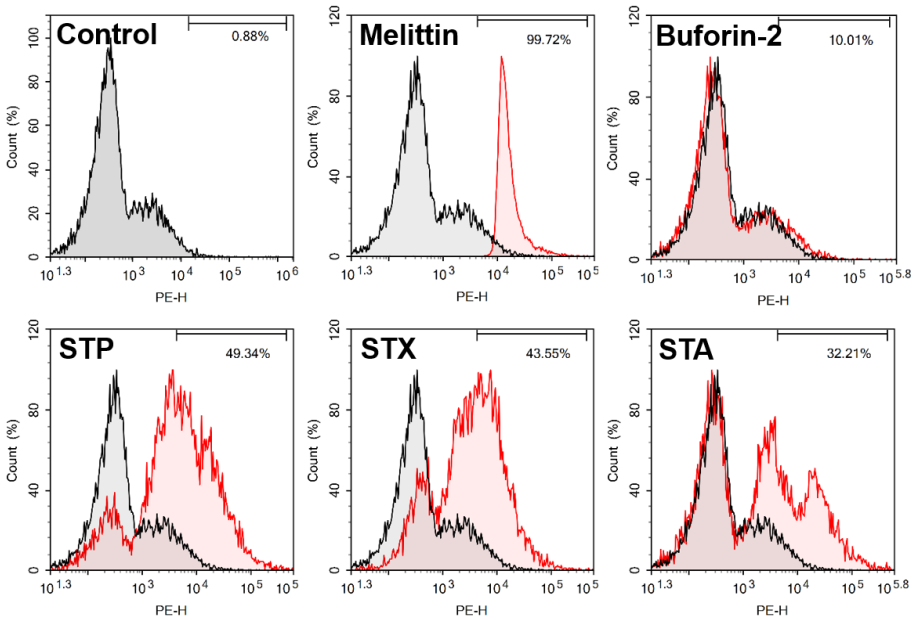

Figure 9. Interaction of STP, STX and STA with membranes. Membrane integrity disruption of MDRPA (CCARM 2095) in presence of peptides (1 × MIC), measured by an increase in fluorescent intensity of propidium iodide (PI). The control was processed without peptides.

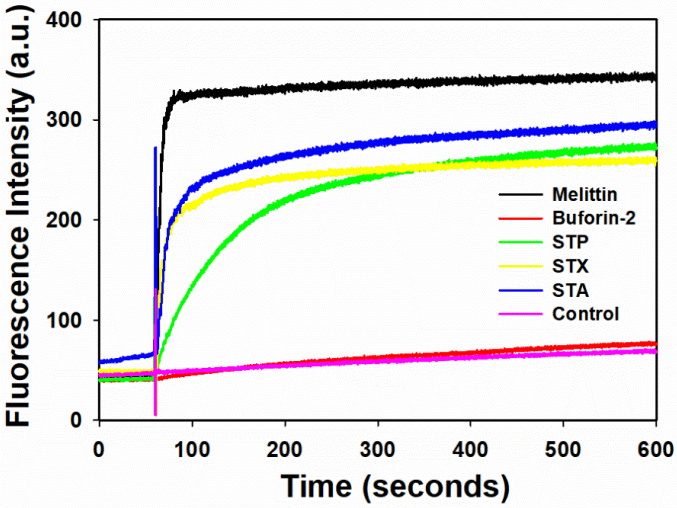

Figure 10. Calcein leakage induced by the STP, STX, and STA against large unilamellar vesicles (LUVs) composed of Phosphatidylethanolamine (PE)/phosphatidylglycerol (PG) (1:1, w/w).

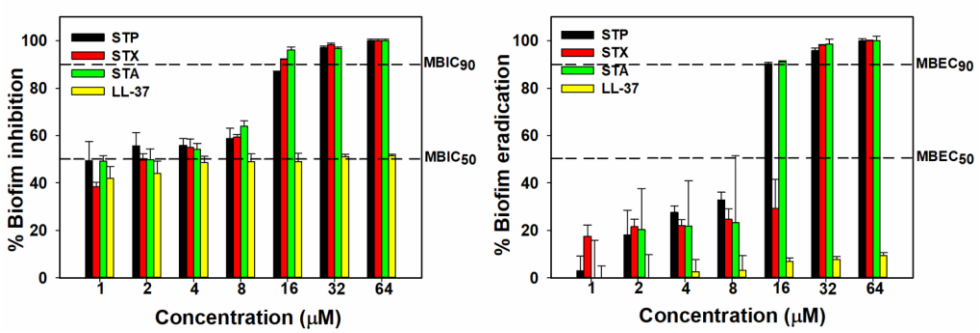

Figure 11. Inhibitory effect of STP, STX, and STA on multidrug-resistant Methicillin-resistant *Staphylococcus aureus* (MRSA) biofilm formation. MRSA (CCARM 3090) was incubated for 24 hours with indicated concentrations of peptides. After incubation, crystal violet was used to stain the biofilm. The stain was dissolved in 95% ethanol, and absorbance at 600 nm (OD_{600}) was measured.

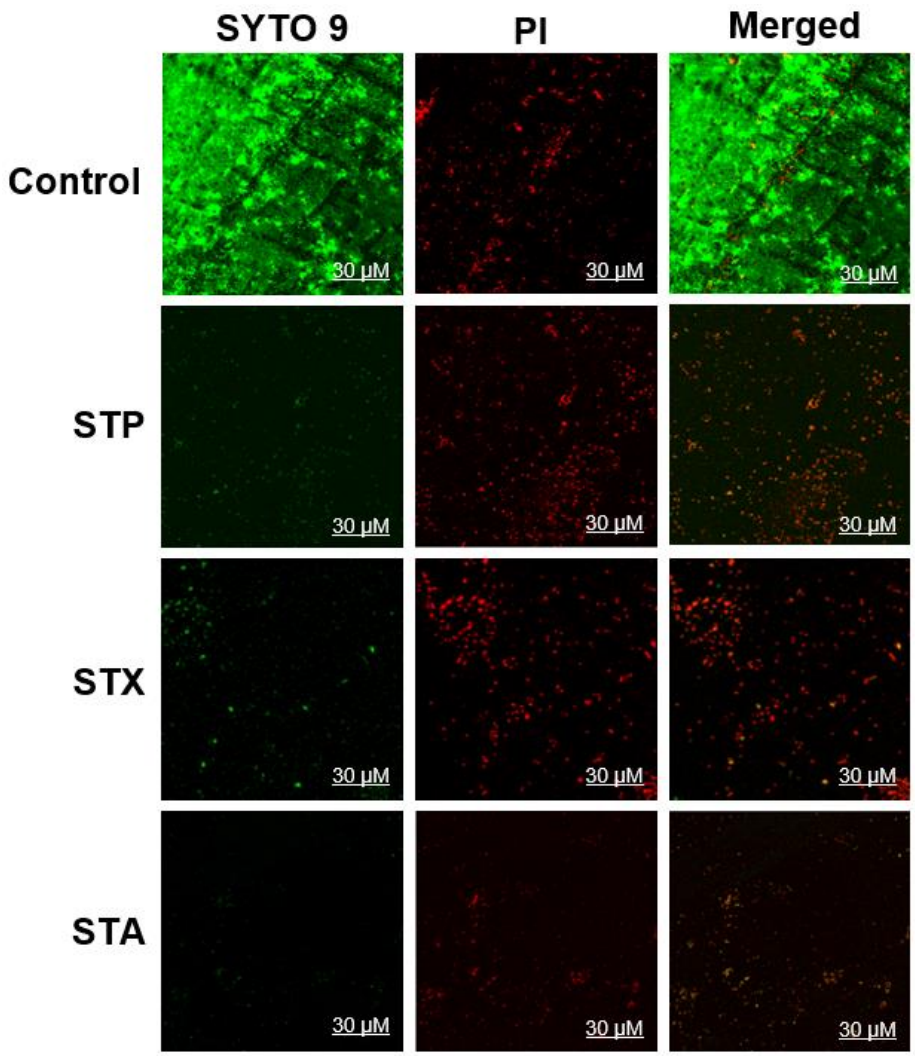

Figure 12. Confocal laser scanning microscopy (CLSM) was used to evaluate biofilm eradication effect of STP, STX, and STA against MRSA. Biofilms were visualized with live/dead bacterial viability staining kit (SYTO 9/PI). Live and dead cells are indicated by green fluorescence (SYTO 9) and red fluorescence (PI), respectively. Scale bar was 30 μM.

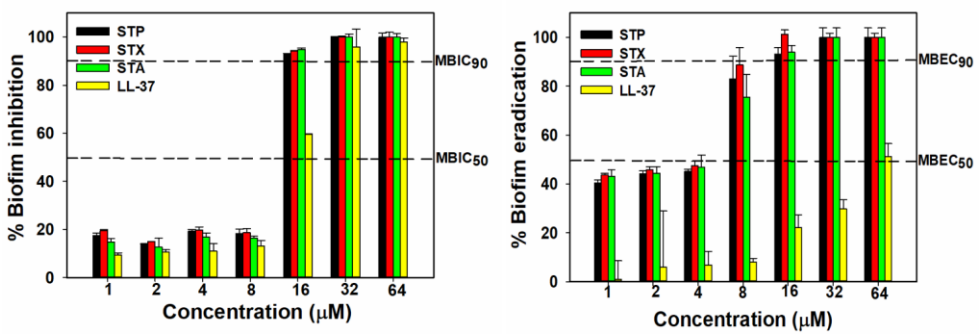

Figure 13. Inhibitory effect of STP, STX, and STA on multidrug-resistant *Pseudomonas aeruginosa* (MDRPA) biofilm formation. MDRPA (CCARM 2095) was incubated for 24 hours with indicated concentrations of peptides. After incubation, crystal violet was used to stain the biofilm. The stain was dissolved in 95% ethanol, and absorbance at 600 nm (OD_{600}) was measured.

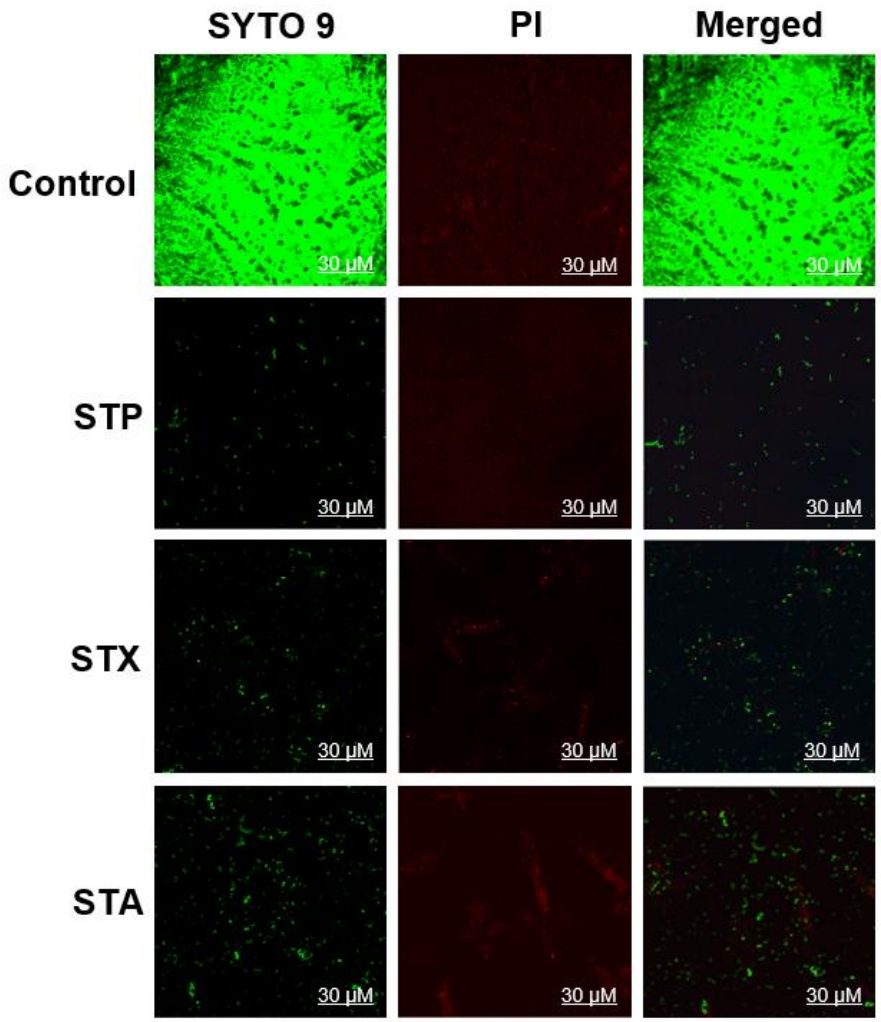

Figure 14. Confocal laser scanning microscopy (CLSM) was used to evaluate biofilm eradication effect of STP, STX, and STA against MDRPA. Biofilms were visualized with live/dead bacterial viability staining kit (SYTO 9/PI). Live and dead cells are indicated by green fluorescence (SYTO 9) and red fluorescence (PI), respectively. Scale bar was 30 μM.

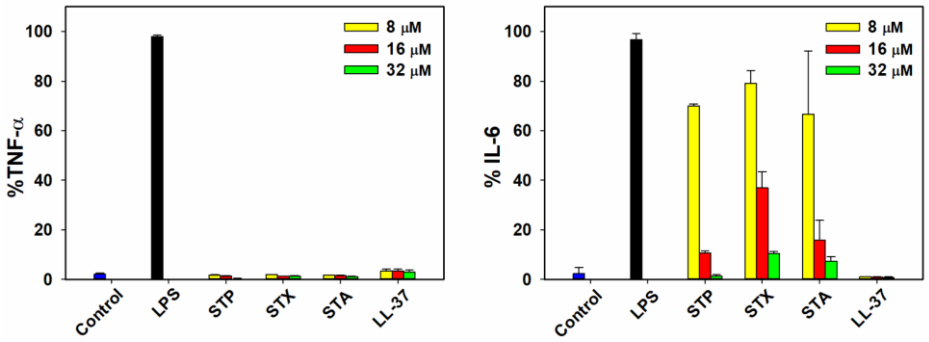

Figure 15. Anti-inflammatory activity STP, STX, and STA. Effects of STP, STX, and STA with control peptide LL-37 on TNF-*α*, and IL-6 in LPS-stimulated macrophage RAW264.7 cells. The concentrations of peptides used for this experiment were 8 μM to 32 μM.

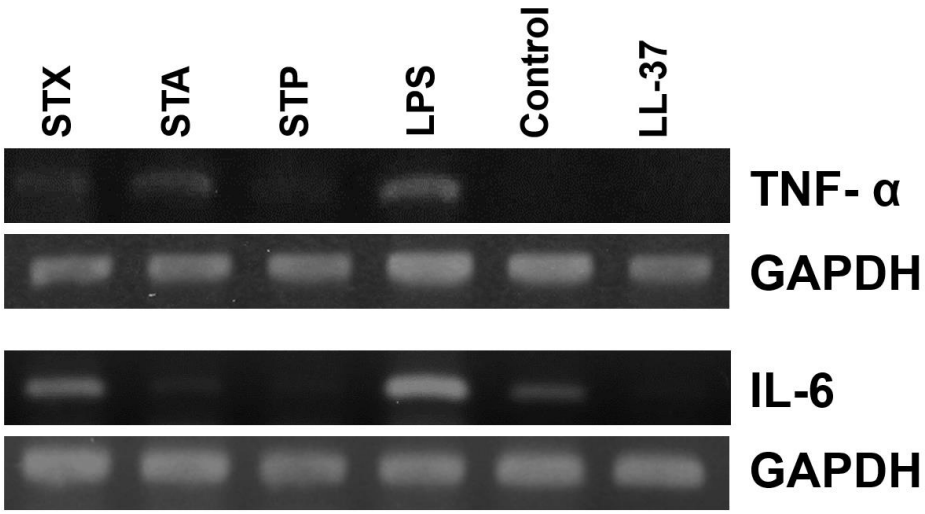

Figure 16. Effects of STP, STX, and STA on mRNA expression of tumor necrosis factor (TNF)-*α*, interleukin (IL)-6 in lipopolysaccharide (LPS)-stimulated RAW264.7 cells. RAW264.7 cells (5×10^5 cells/well) were incubated with peptides at 16 μM concentrations in the presence of LPS (20 ng/ml) for 3 hours (for TNF-*α*, IL-6). Total RNA was isolated and analyzed to determine mRNAs levels of TNF-*α*, IL-6 using reverse transcription-polymerase chain reaction (RT-PCR).

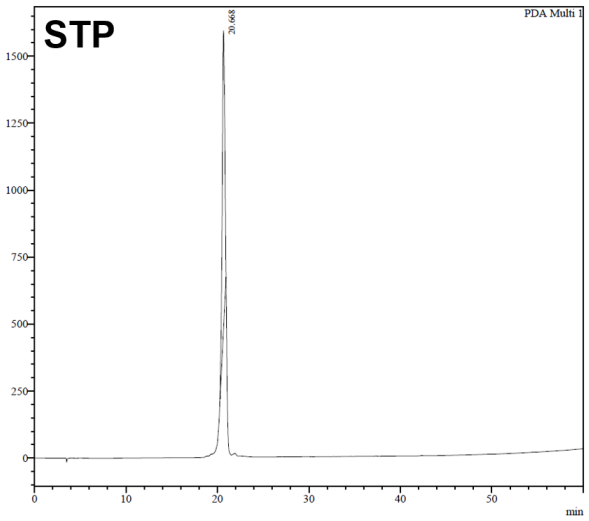

Figure S1. Analytical RP-HPLC profiles of Synthetic STP. Peptides were eluted for 60 minutes with a flow rate of 1.0 mL/min by analytical RP-HPLC on a C_{18} column (5 mm; 4.6 mm × 250 mm; Vydac) using a gradient of buffer B (0.05% TFA in CH_3CN/H_2O 90:10 v/v) in buffer A (0.05% TFA in H_2O).

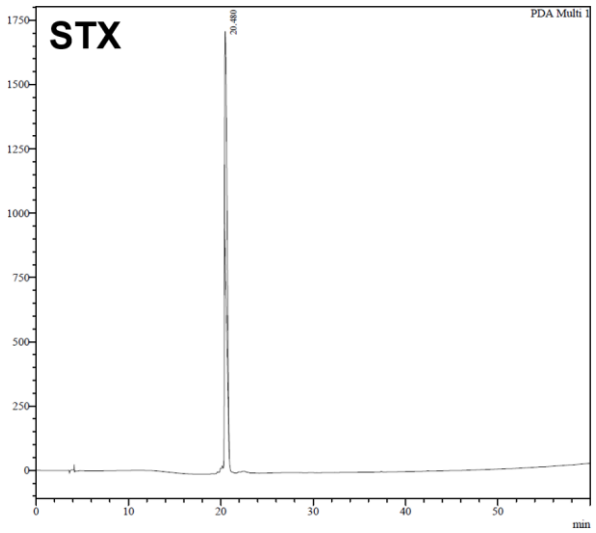

Figure S2. Analytical RP-HPLC profiles of Synthetic STX. Peptides were eluted for 60 minutes with a flow rate of 1.0 mL/min by analytical RP-HPLC on a C_{18} column (5 mm; 4.6 mm × 250 mm; Vydac) using a gradient of buffer B (0.05% TFA in CH_3CN/H_2O 90:10 v/v) in buffer A (0.05% TFA in H_2O).

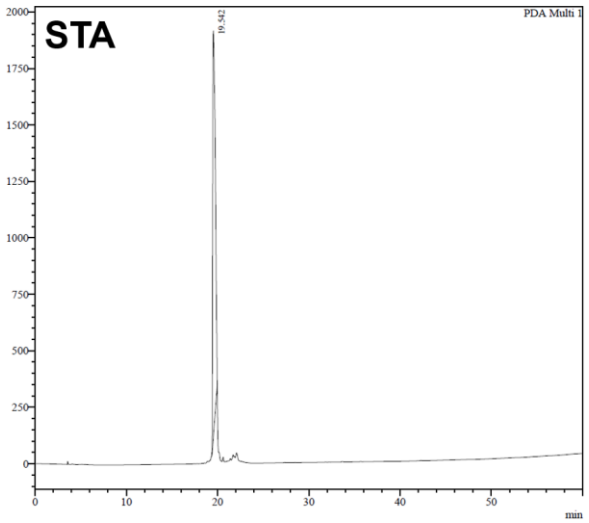

Figure S3. Analytical RP-HPLC profiles of Synthetic STA. Peptides were eluted for 60 minutes with a flow rate of 1.0 mL/min by analytical RP-HPLC on a C_{18} column (5 mm; 4.6 mm × 250 mm; Vydac) using a gradient of buffer B (0.05% TFA in CH_3CN/H_2O 90:10 v/v) in buffer A (0.05% TFA in H_2O).

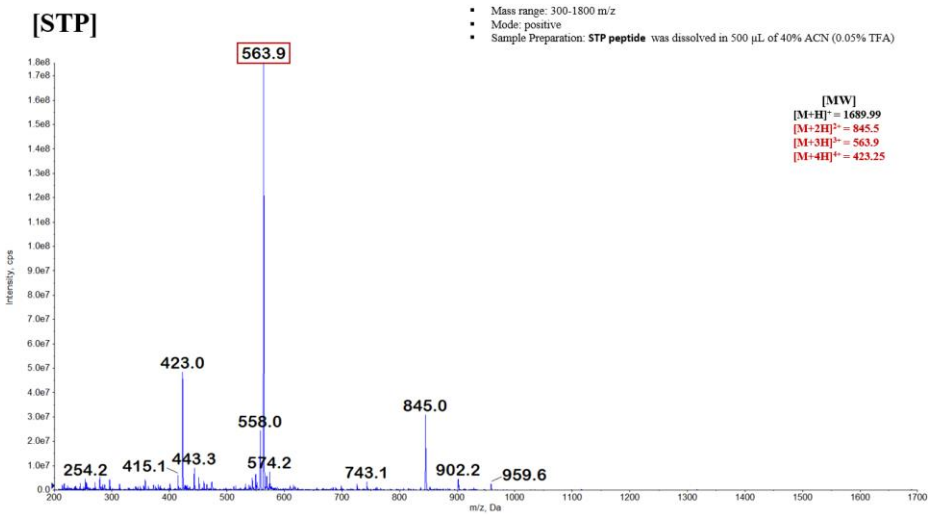

Figure S4. Electrospray ionization-mass spectrometry (ESI-MS) spectra of Synthetic STP.

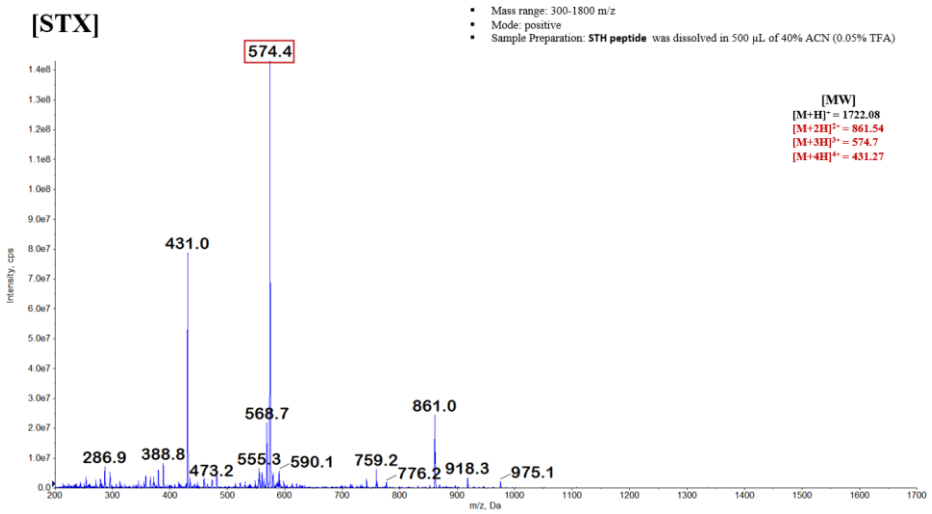

Figure S5. Electrospray ionization-mass spectrometry (ESI-MS) spectra of Synthetic STX.

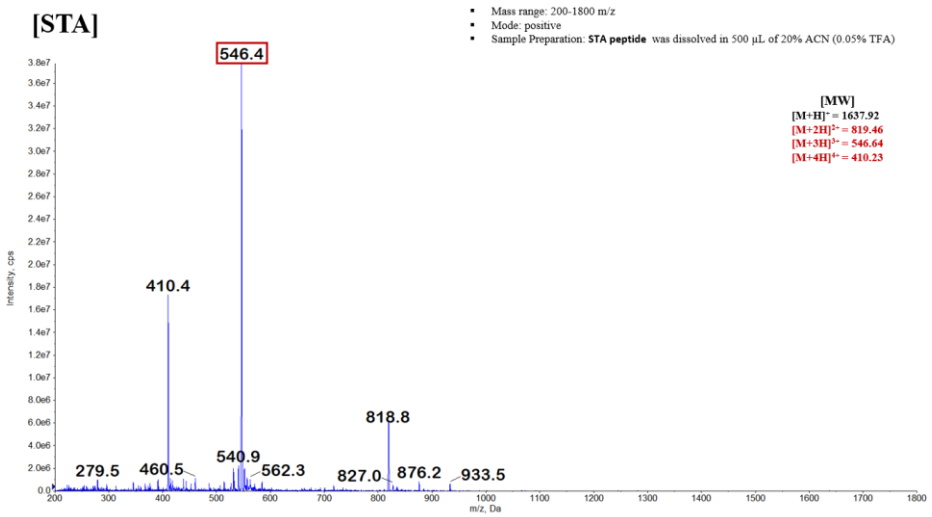

Figure S6. Electrospray ionization-mass spectrometry (ESI-MS) spectra of Synthetic STA.

References

[1] S. Tomczyk, V. Zanichelli, M.L. Grayson, A. Twyman, M. Abbas, D. Pires, B. Allegranzi, S. Harbarth, Control of carbapenem-resistant enterobacteriaceae, acinetobacter baumannii, and pseudomonas aeruginosa in healthcare facilities: a systematic review and reanalysis of quasi-experimental studies. *Clin. Infect Dis.* 68 (2019) 873-884

[2] C. Willyard, The drug-resistant bacteria that pose the greatest health threats. *Nature.* 543 (2017), 15

[3] K.H. Luepke, K.J. Suda, H. Boucher, R.L. Russo, M.W. Bonney, T.D. Hunt, J.F. Mohr. 3rd, Past, present, and future of antibacterial economics: increasing bacterial resistance, limited antibiotic pipeline, and societal implications. *Pharmacotherapy*. 37 (2017), 71-84

[4] R.E.W. Hancock, H.G. Sahl, Antimicrobial and host-defense peptides as new anti-infective therapeutic strategies. *Nat Biotechnol.* 24 (2006), 1551-1557

[5] M. Zasloff, Antimicrobial peptides of multicellular organisms. *Nature.* 415 (2002), 389-395

[6] D.M. Easton, A. NiJnik, M.L. Mayer, R.E.W. Hancock, Potential of immunomodulatory host defense peptides as novel anti-infectives. *Trends Biotechnol.* 27 (2009), 582-590

[7] Mariam Rima, Mohamad Rima, Z. Fajloun, J.-M. Sabatier, B. Bechinger, T. Naas, Antimicrobial Peptides: A Potent Alternative to Antibiotics. *Antibiotics.* 10 (2021), 1095

[8] L.R. Mclean, K.A. Hagaman, T.J. Owen, J.L. Krstenansky, Minimal peptide length for interaction of amphipathic alpha-helical peptides with phosphatidylcholine liposomes, *Biochemistry*. 30 (1991), 31-37

[9] Clinical, L.S. Institute, Methods for dilution antimicrobial susceptibility tests for bacteria that grow aerobically; Approved standard-tenth edition, CLSI Document M07-A10, (2015), 950

[10] G. Rajasekaran, S.D. Kumar, S. Yang, S.Y. Shin, The design of a cell-selective fowlicidin-1-derived peptide with both antimicrobial and anti-inflammatory activities, *Eur J Med Chem*. 182 (2019), 111623

[11] B. Jacob, Y. Kim, J.K. Hyun, et al., Bacterial killing mechanism of sheep myeloid antimicrobial peptide-18 (SMAP-18) and its Trp-substituted analog with improved cell selectivity and reduced mammalian cell toxicity, *Amino Acids*. 46 (2014) 187-198

[12] R.I. Lehrer, A. Barton, K.A Daher, S.S. Harwig, Interaction of human defensins with *Escherichia coli.* mechanism of bactericidal activity, *J. Clin. Invest*. 84 (1989) 553-561

[13] C.L. Friedrich, D. Moyles, T.J. Beveridge, R.E.W. Hancock, Antibacterial action of structurally diverse cationic peptides on gram-positive bacteria, *Antimicrob Agents Chemother*. 44 (2000) 2086-2092

[14] E.Y. Kim, G. Rajasekaran, S.Y. Shin, LL-37-derived short antimicrobial peptide KR-12-a5 and its d-amino acid substituted analogs with cell selectivity, anti-biofilm activity, synergistic effect with conventional antibiotics, and anti-inflammatory activity, *Eur J Med. Chem.* 136 (2017) 428-441

[15] G. Rajasekaran, S.D. Kumar, S. Yang, S.Y. Shin, The design of a cell-selective fowlicidin-1-derived peptide with both antimicrobial and anti-inflammatory activities, *Eur J Med Chem.* 182 (2019), 111623

[16] A.A. Strömstedt, M. Pasupuleti, A. Schmidtchen, M. Malmsten, Evaluation of strategies for improving proteolytic resistance of antimicrobial peptides by using variants of EFK17, an internal segment of LL-37. *Antimicrob Agents Chemother*. 53 (2009) 593-602

[17] A. Basak, Y. Abouelhassan, R. Zuo, H. Yousaf, Y. Ding, R.W. Huigens, Antimicrobial peptide-inspired NH125 analogues: bacterial and fungal biofilm-eradicating agents and rapid killers of MRSA persisters. *Org Biomol Chem*. 15 (2017), 5503-5512

[18] J.J. Harrison, C.A. Stremick, R.J. Turner, N.D. Allan, M.E. Olson, H. Ceri, Microtiter susceptibility testing of microbes growing on peg lids: a miniaturized biofilm model for high-throughput screening. *Nature protocols*. 5 (2010), 1236-1254

[19] F. Silva, O. Lourenço, J.A. Queiroz, F.C. Domingues, Bacteriostatic versus bactericidal activity of ciprofloxacin in Escherichia coli assessed by flow cytometry using a novel far-red dye, *J. antibiotics*. 64 (2011) 321-325